DE GRUYTER OPEN

GEOCHRONOMETRIA 44 (2017): 352–365
DOI 10.1515/geochr-2015-0077

Available online at
http://www.degruyter.com/view/j/geochr

POST-IR IRSL DATING OF K-FELDSPAR FROM LAST INTERGLACIAL MARINE TERRACE DEPOSITS ON THE KAMIKITA COASTAL PLAIN, NORTHEASTERN JAPAN

KAZUMI ITO[1], TORU TAMURA[1] and SUMIKO TSUKAMOTO[2]

[1]*Geological Survey of Japan, National Institute of Advanced Industrial Science and Technology (AIST), Ibaraki, Japan*
[2]*Leibniz Institute for Applied Geophysics (LIAG), S3: Geochronology and Isotope Hydrology, Hannover, Germany*

Received 26 December 2016 Accepted 8 September 2017

Abstract: To establish a suitable luminescence dating protocol for marine terrace deposits in Japan, we tested the applicability of K-feldspar post-infrared (IR) infrared stimulated luminescence (IRSL) (pIRIR) dating using a marine isotope stage (MIS) 5e terrace deposit from the Kamikita coastal plain (NE Japan), where independent age control from a tephra is available. One of the most commonly used pIRIR signals, measured at 290°C with the first IR stimulation temperature at 50°C ($pIRIR_{50/290}$), faded with a mean g_{2days} value of 1.94 ± 0.19%/decade. In contrast, the pIRIR signal with a higher first IR stimulation temperature of 200°C ($pIRIR_{200/290}$) had a much lower fading rate (g_{2days} = 0.16 ± 0.49%/decade). The average fading-uncorrected and -corrected $pIRIR_{200/290}$ ages of MIS 5e subtidal sediments obtained from two sampling sites were 126 ± 3 ka and 132 ± 2 ka, which is in good agreement with the independent age control. We conclude that is it is now possible to use pIRIR protocol to estimate the ages of not only marine terraces formed during MIS 5 substages (5a, 5c) but also of older marine terraces, for which age evidence is limited.

Keywords: post-IR IRSL dating, K-rich feldspar, fading correction, marine terrace, MIS 5e.

1. INTRODUCTION

Late Pleistocene marine terraces formed during interglacial sea-level highstands are widely distributed across the Japanese islands. Tephrochronology has been used to correlate these terraces with marine isotope stages (MIS) (Machida and Arai, 2003). Ages of marine terraces formed during the last interglacial (MIS 5e; 123 ± 7 ka) are well defined in many places (e.g., Koike and Machida, 2001) by widely distributed marker tephras. Marker tephras, such as Ontake Pm1 (On-Pm1, 95.7 ± 5.3 ka, Aoki *et al*., 2008) and Toya (106 ka, Shirai *et al*., 1997; 112–115 ka, Machida and Arai, 2003; 104 ± 15 ka to 118 ± 15 ka, Ganzawa and Ike, 2011) in eastern Japan, and Aso-4 (86.8–87.3 ka, Aoki, 2008) and Sanbe-Kisuki (SK, 100–115 ka, Shiraishi *et al*., 1992) in western Japan (Machida and Arai, 2003), have helped to establish the chronology of these MIS 5e terraces. However, marker tephras are not always found in marine terrace deposits; thus, the chronology of marine terraces has often been determined by counting interglacial deposits backward from MIS 5e. The dating of marine terraces is particularly important for evaluating long-term vertical crustal movements, and a suitable, universally applicable age determination method for this purpose is desirable.

Optically stimulated luminescence (OSL) dating of quartz has been widely applied to date coastal and marine sediments (Jacobs, 2008). In Japan, Tanaka *et al*. (1997) successfully used the multiple-aliquot additive dose (MAAD) method to determine a quartz OSL age for a

Corresponding author: K. Ito
e-mail: kazumi-itou@aist.go.jp

ISSN 1897-1695 (online), 1733-8387 (print)

marine terrace on the Noto Peninsula corresponding to MIS 5e. Barreto *et al*. (2002) also used the MAAD quartz OSL method to successfully date marine terraces in northeastern Brazil formed during MISs 7 and 5e. Choi *et al*. (2003) dated marine terrace sediments on the Korean Peninsula by using the quartz single-aliquot regenerative dose (SAR) method and obtained ages ranging from 50 ka to 70 ka, which are younger than the expected last interglacial age. The equivalent dose (D_e) of the OSL signal, however, is commonly close to saturation in samples from the last interglacial period, except when the environmental dose rate is low (Murray and Funder, 2003; Pawley *et al*., 2008; Pascucci *et al*., 2014). K-feldspar displays higher dose saturation levels than quartz, so the K-feldspar SAR method is suitable for dating older sediments. Pedoja *et al*. (2006a, 2006b) used the SAR method to obtain infrared stimulated luminescence (IRSL) ages of feldspar from marine terraces in Ecuador and Peru. Because luminescence signals of feldspars are known to decrease after burial as a result of tunneling (anomalous fading) (Aitken, 1985), they corrected their ages for fading following Huntley and Lamothe (2001) and obtained fading-corrected ages corresponding to MISs 5e, 7, and 9.

Thomsen *et al*. (2008) found that the IRSL signal measured at an elevated temperature of 225°C after an initial low-temperature IRSL measurement at 50°C (IR_{50}; the subscript refers to the measurement temperature) is much more stable (fades less) than the IR_{50} signal. This signal is called a post-IR IRSL (pIRIR) signal; hereafter, the first and second stimulation temperatures are shown as a subscript (e.g., $pIRIR_{50/225}$). The pIRIR method effectively minimizes anomalous fading and has been applied to the determination of depositional ages older than the limit of quartz OSL age (e.g., Buylaert *et al*., 2009; Thiel *et al*., 2010, 2015; Kars *et al*., 2012). Moreover, pIRIR signals obtained at the higher measurement temperature of 290°C ($pIRIR_{50/290}$; Thiel *et al*., 2011a, 2011b, 2012; Buylaert *et al*., 2012, 2013, 2015) and multiple elevated temperature (MET) pIRIR signals obtained at measurement temperatures higher than 250°C (Li and Li, 2011, 2012; Li *et al*., 2014) have been found to be more stable and often do not require anomalous fading correction. Buylaert *et al*. (2012) and Roberts (2012) suggested that low fading rates (g-value: <1.0–1.5%/decade) may be an artifact of laboratory measurement, and that such rates may have a negligible effect on measured ages. Thiel *et al*. (2012, 2015) have used this sufficiently stable $pIRIR_{50/290}$ signal to determine the ages of marine terrace deposits. Thiel *et al*. (2012) demonstrated the feasibility of using the $pIRIR_{50/290}$ protocol to determine the ages of marine terrace deposits as old as MIS 13 in Tunisia. Thiel *et al*. (2011a) assumed that no fading correction of $pIRIR_{50/290}$ signals from fine-grained polymineral samples from tephric loess in Japan was needed. Additionally, Zander and Hilgers (2013) reported that the $pIRIR_{50/290}$ signal is stable enough for a dose estimation even as high as 1600 Gy, and they could determine ages as far back as the Brunhes-Matuyama reversal from fine polymineral grains from Lake El'gygytgyn, Siberia. Thiel *et al*. (2015) found that the $pIRIR_{50/225}$ signal from coarse-grained K-feldspar from the Oga Peninsula, northeastern Japan, displayed a non-negligible fading rate (1.3–2.3%/decade), whereas Buylaert *et al*. (2012) showed that the $pIRIR_{50/290}$ signal from the same material was sufficiently stable. Additionally, Thiel *et al*. (2015) showed that fading-corrected $pIRIR_{50/225}$ ages (corrected using the approach of Huntley and Lamothe, 2001) and uncorrected $pIRIR_{50/290}$ ages were consistent with one another and with independent age control.

In this study, we investigated $pIRIR_{290}$ signals obtained after different first IR stimulation temperatures from K-feldspar from marine terrace deposits in northeastern Japan that formed during the last interglacial. For each different first IR stimulation temperature, we measured D_e values, dose recovery ratios, residual doses, and g-values, and then calculated fading-uncorrected and -corrected ages. To select the most suitable signal, we then compared the pIRIR ages with ages of the marine terrace MIS5e reported by Miyauchi (1987) and Koike and Machida (2001). The age of MIS 5e is based on Lisiecki and Raymo (2005) (123 ± 7 ka).

2. GEOLOGICAL SETTING AND SAMPLING

Kamikita coastal plain

The Kamikita coastal plain, which lies along the Pacific coast at the northeastern end of Honshu Island, is about 50 km long and 30 km wide (**Fig. 1**). The plain has six marine terrace surfaces, named the Higher (Fukuromachi) (elevation, 110–220 m), Shichihyaku (90–110 m), Tengutai (45–80 m), Takadate (30–40 m), Nejo (10–15 m), and Shibayama (<10 m) surfaces, and two levels of fluvial terraces, the Shichinohe and Sanbongi (<5 m) surfaces (Miyauchi, 1985, 1987; Koike and Machida, 2001). The northeastern part of the Kamikita plain is occupied by Lake Ogawara, an irregularly shaped body of water that is generally elongated parallel to the coast. Seaward of the lake, only the Takadate terrace and the two fluvial terraces have been mapped. The Holocene plain is distributed only along the rivers draining into the lake and the lake's outlet to the sea, and is not extensively developed along the modern shoreline.

The age of the Takadate terrace is constrained by the presence of the Toya tephra, which has been dated to 112–115 ka by a combination of fission track dating, thermoluminescence (TL) dating, and stratigraphy (Machida and Arai, 2003), and to 104 ± 15 to 118 ± 15 ka by red TL dating (Ganzawa and Ike, 2011). Shirai *et al*. (1997) and Matsuura *et al*. (2014) reported that based on marine sediment core the Toya tephra was erupted during MIS 5d (106 ka). The Toya tephra is found in the terrigenous upper part of the Takadate terrace deposits; thus, the underlying subtidal facies deposits are thought to

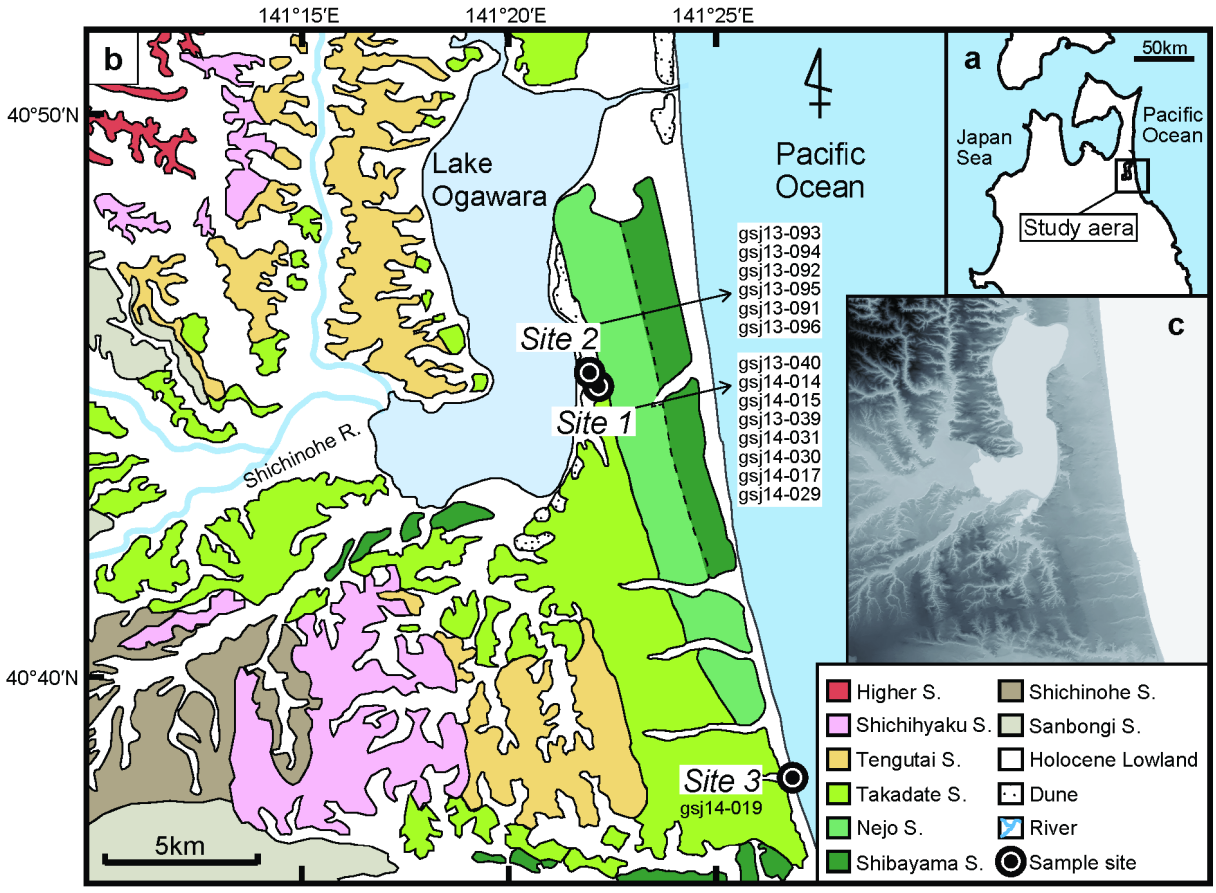

Fig. 1. *(a) Location map of the Kamikita coastal plain, northeastern Japan. (b) Map showing the distribution of Late and Middle Pleistocene marine terraces and sampling sites (after Miyauchi, 1985, 1987). In the legend, surface is abbreviated as "S" The elevation range of each terrace is given in the text. (c) Digital elevation model of the Kamikita coastal plain based on 10-m-grid data from the Geospatial Information Authority of Japan. Lighter grays indicate lower elevations, and darker grays and black indicate higher elevations.*

have formed during the last interglacial sea-level highstand (123 ± 7 ka). Although their ages are less well constrained, the Higher, Shichihyaku, and Tengutai terraces are presumed to have formed during older interglacial highstands, MIS 11, 9, and 7, respectively, whereas the Nejo (MIS 5c) and Shibayama (MIS 5a) terraces are younger than the Takadate terrace. Kuwabara (2009) correlated the Shichihyaku and Tengutai terraces with MIS 9 and 7, respectively, on the basis of phytolith evidence. The terrace sequence is thought to reflect both global sea-level changes and steady tectonic regional uplift caused by east–west horizontal compression during the Late Pleistocene (e.g., Miyauchi, 1985, 1987).

Outcrops and sampling

We investigated two outcrops (sites 1 and 2) at the landward edge of the Takadate terrace, facing Lake Ogawara (**Fig. 1**). Depositional facies of the outcrops were defined and interpreted based on sedimentary structures and grain size. The elevations of the facies boundaries were measured with a virtual reference station GPS (Leica Viva GS08plus, Leica). These outcrops are 330 m apart and appear to expose laterally continuous deposits. The depositional succession beneath the Takadate terrace consists of lower subtidal facies and an upper terrigenous deposit, both of which were sampled. Light-tight black PVC tubes 15 cm long and 5 cm in diameter were hammered into the outcrop to sample sediment unexposed to light. Modern beach sand (sample gsj14-019) was collected at site 3 (**Fig. 1**) to determine the residual dose. This sample was obtained from *ca.* 10 cm depth by using the same type of tube.

Site 1

The subtidal facies at site 1 consists of fine to coarse sand containing granules and pebbles (**Fig. 2**). The lower part of the unit, 8 m thick, consists of cross-laminated gravelly coarse sand alternating with cross-laminated fine to medium sand. The coarse sand contains wave dunes and the fine sand contains burrows. This assemblage reflects the dominance of storm-wave sedimentation in the lower shoreface (Walker and Plint, 1992; Cummings

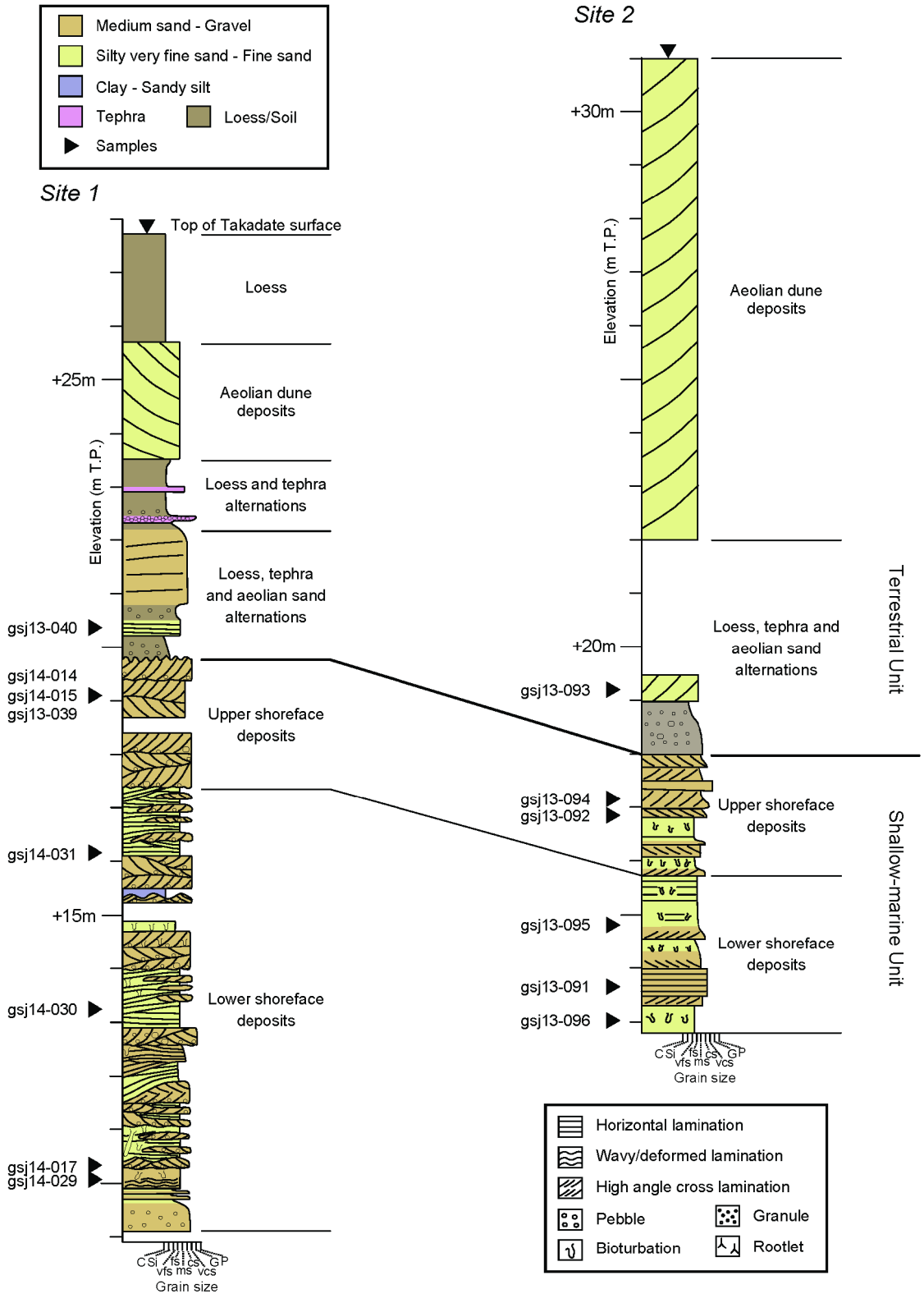

Fig. 2. *Columnar sections from sites 1 and 2. Grain size is categorized into clay, silt, very fine sand, fine sand, medium sand, coarse sand, very coarse sand, granules, and pebbles (C, Si, vfs, fs, ms, cs, vcs, G, and P, respectively). The bold horizontal line represents the erosional surface between the terrestrial and subtidal facies deposits. T.P. (Tokyo Peil) is the standard datum for elevation measurements in Japan.*

et al., 2009). The upper part of the unit, 2.5 m thick, is composed of trough cross-laminated coarse sand containing granules and pebbles, and it overlies the lower part of the unit with an erosional contact. The cross-lamination is indicative of the sedimentation of dunes in the upper shoreface (Clifton, 2006). The generally coarsening-upward succession in the shallow-marine unit thus consists of regressive shoreface deposits (Walker and Plint, 1992). The erosional upper boundary of the unit at 19.8 m elevation implies that overlying deposits were removed from the upper shoreface and foreshore by erosion.

The terrigenous unit at site 1 consists of alternating sand and brownish silt. The silt layers are poorly sorted and contain sand and granules, and their brownish color indicates that they are loess beds or paleosols. A few unidentified tephra layers are intercalated with the silt layers. The sand layers are 30 cm to 200 cm thick and characterized by well-defined cross- to horizontal laminations. A 2-m-thick sand layer in the upper part of the unit exhibits aeolian dune stratification dipping eastward in the direction of the winter monsoon winds in this region. Other sand layers also probably represent aeolian dunes or sand sheets, because they are interbedded with paleosols.

We took four sediment samples for luminescence dating from different levels of the lower shoreface deposits (gsj14-017, gsj14-029, gsj14-030, and gsj14-031), three samples from one level of the upper shoreface deposits (gsj13-039, gsj14-014, and gsj14-015), and one sample from aeolian sand deposits (gsj13-040).

Site 2

The subtidal facies at site 2 consists of coarsening-upward regressive shoreface deposits similar to those at site 1. Its erosional upper boundary is at 18.0 m elevation, suggesting slightly deeper erosion than at site 1. The terrigenous unit, as at site 1, is composed of aeolian sand and brownish paleosols, but its uppermost part is dominated by 9-m-thick aeolian dune deposits showing east-dipping cross-lamination. The same aeolian dune extends along the eastern shoreline of Lake Ogawara (**Fig. 1**; Miyauchi, 1985, 1987).

Samples for luminescence dating were taken from three levels of the lower shoreface deposits (gsj13-091, gsj13-095, and gsj13-096), from two levels of the upper shoreface deposits (gsj13-092 and gsj13-094), and from one level of the aeolian sand deposits (gsj13-093).

Expected age of subtidal facies deposits

The two subtidal facies, upper shoreface and lower shoreface, accumulated under different water depths and during different time periods and thus have different sedimentation ages. In Denmark, Fruergaard *et al*. (2015) confirmed that samples from subtidal facies are completely bleached by using OSL ages of Holocene samples, which increase with depth in direct correspondence to the sedimentation age of each sample. During the Holocene, the sedimentation rate of beach shorefaces has been rapid, with sedimentary successions 10–15 m thick forming in only 2000 years (e.g., Tamura *et al*., 2007). On longer Pleistocene timescales (e.g., 100 ka), a 2000-year age difference comprises only 2% of a sample's age. Thiel *et al*. (2015) illustrated a depth profile of $pIRIR_{50/225}$ ages of samples from subtidal facies (Thiel *et al*., 2015; their Fig. 13); in this profile, the $pIRIR_{50/225}$ ages of samples from subtidal facies collected at heights 5 m to 25 m do not increase with depth. Therefore, we do not expect the ages of our samples from the subtidal facies to increase with depth but to concentrate at about 123 ± 7 ka, the age of the MIS 5e sea-level highstand.

3. SAMPLE PREPARATION, MEASUREMENT APPARATUS, AND DOSE-RATE CALCULATION

All samples were processed and measured at the luminescence laboratory of the Geological Survey of Japan. Sediment within 3 cm from each end of the tube, which may have been exposed to sunlight during sampling, was removed and used for measuring moisture content and dosimetry. The remaining sediment was processed to extract coarse grains of K-rich feldspar. The samples were treated with 10% HCl and 10% H_2O_2 to dissolve carbonate and organic matter, respectively, and then screened using 180 μm and 250 μm mesh sieves. Finally, the K-rich feldspar fraction (ρ = 2.53–2.58 g/cm^3; Aitken, 1998) was isolated by using sodium polytungstate. The feldspar grains were then mounted in aliquots with a diameter of 8.0 mm by using silicone oil on stainless steel disks with a diameter of 9.8 mm.

Luminescence signals were measured with a TL-DA-20 automated Risø reader equipped with infrared LEDs for stimulation (145 mW/cm^2; central wavelength, 870 nm) and a $^{90}Sr/^{90}Y$ beta source (dose rate, *ca.* 0.19 Gy/s) for laboratory irradiation, which was calibrated by using stainless steel and 180-250 μm calibration quartz from Risø. Emissions in the blue–violet region, which are dominantly K-feldspar emissions (Huntley *et al*., 1991), were measured through Schott BG3 (thickness, 3 mm), BG39 (2 mm), and GG400 (3 mm) filters.

The contributions of natural radioisotopes and cosmic radiation were considered in the determination of the annual dose rate. After mixing and homogenization of the dried sample, radioisotope concentrations were measured by inductively coupled plasma mass spectrometry and converted to dose rates by using the conversion factors of Guérin *et al*. (2011) (**Table 1**). The uncertainty of the radioisotope concentrations was assumed to be ±5%. Water content was estimated from the mean of the natural and saturated water contents and expressed as weight of water / weight of dry sediment, with a ±5% uncertainty. The saturated water content of 31.0% was calculated from the mean saturated water content of four samples (gsj13-039, gsj13-040, gsj13-093, and gsj13-094) and

Table 1. *Radioisotope concentration, water content, cosmic ray and dose-rate for sediment samples. Listed water content was natural value. The water content for dose rate calculation was estimated from the mean of natural and saturated (31.0%) water contents. For details see main text.*

Sample	Depth (m)	Radioisotope concentraion				Water Content (%)	Cosmic Dose Rate (Gy/ka)	Dose-rate (Gy/ka)
		K (%)	Rb (ppm)	Th (ppm)	U (ppm)			
Site 1								
gsj13-040	7.40	0.62 ± 0.06	20.8 ± 2.1	1.35 ± 0.14	0.38 ± 0.04	3.0	0.10	1.57 ± 0.12
gsj14-014	8.30	0.68 ± 0.07	23.2 ± 2.3	1.55 ± 0.16	0.44 ± 0.04	7.3	0.09	1.62 ± 0.12
gsj14-015	8.30	0.72 ± 0.07	23.1 ± 2.3	1.85 ± 0.19	0.48 ± 0.05	9.3	0.09	1.67 ± 0.12
gsj13-039	8.30	0.77 ± 0.08	19.9 ± 2.0	1.60 ± 0.16	0.44 ± 0.04	11.3	0.09	1.67 ± 0.12
gsj14-031	11.54	0.83 ± 0.08	24.9 ± 2.5	1.67 ± 0.17	0.52 ± 0.05	16.1	0.07	1.70 ± 0.12
gsj14-030	14.47	0.88 ± 0.09	24.1 ± 2.4	2.09 ± 0.21	0.60 ± 0.06	20.2	0.06	1.75 ± 0.12
gsj14-017	17.60	0.69 ± 0.07	23.1 ± 2.3	2.46 ± 0.25	0.46 ± 0.05	15.7	0.04	1.60 ± 0.11
gsj14-029	17.61	0.78 ± 0.08	22.9 ± 2.3	2.34 ± 0.23	0.74 ± 0.07	24.1	0.04	1.69 ± 0.12
Site 2								
gsj13-093	11.84	0.50 ± 0.05	19.2 ± 1.9	1.63 ± 0.16	0.46 ± 0.05	11.4	0.07	1.44 ± 0.10
gsj13-094	13.80	0.52 ± 0.05	18.0 ± 1.8	1.30 ± 0.13	0.37 ± 0.04	11.2	0.06	1.41 ± 0.10
gsj13-092	14.08	0.71 ± 0.07	25.5 ± 2.6	1.93 ± 0.19	0.58 ± 0.06	17.7	0.06	1.61 ± 0.11
gsj13-095	16.07	0.69 ± 0.07	24.9 ± 2.5	1.82 ± 0.18	0.52 ± 0.05	19.2	0.05	1.57 ± 0.11
gsj13-091	17.33	0.55 ± 0.06	22.1 ± 2.2	1.80 ± 0.18	0.47 ± 0.05	10.3	0.05	1.48 ± 0.11
gsj13-096	18.03	0.73 ± 0.07	24.3 ± 2.4	1.94 ± 0.19	0.54 ± 0.05	18.7	0.04	1.60 ± 0.11
Site 3								
gsj14-019	0.10	0.18 ± 0.02	6.2 ± 0.6	0.79 ± 0.08	0.22 ± 0.02	5.9	0.21	1.50 ± 0.10

used for all samples. The α-dose and β-dose attenuation factors were taken from Bell (1980) and Mejdahl (1979), respectively. The relative alpha efficiency (a-value) of K-rich feldspar was set to 0.15 ± 0.05, as assumed by Balescu and Lamothe (1994). The size of the K-feldspar grains was determined to be 221 ± 6 μm by a CAMSIZ-ER apparatus (Retsch Technology). The K content of the feldspar was assumed to be 12.5 ± 0.5% (Huntley and Baril, 1997). The internal U and Th contents were assumed to be zero. No internal α-dose rate contribution from U and Th was considered, referred to the data set shown in Duller (1992). The cosmic dose rate was estimated following Prescott and Hutton (1994).

4. LUMINESCENCE CHARACTERISTICS

Equivalent dose measurement and procedural tests

Using gsj13-039 and gsj13-094, we investigated the characteristics of $pIRIR_{290}$ signals with different first IR stimulation temperatures. The pIRIR stimulation temperature and preheat temperature were fixed at 290°C and 320°C, while the first IR stimulation temperature was varied between 50°C and 250°C with a 50°C increment. The luminescence signal was measured in 0.1-s bins. The decay curves of the five pIRIR signals from gsj13-039 are shown in **Fig. 3a**. The highest intensity was that of the $pIRIR_{50/290}$ signal at *ca.* 11,000 counts in the first 0.1 s, while the $pIRIR_{250/290}$ signal intensity was only *ca.* 400 counts in the first 0.1 s.

Buylaert *et al*. (2012) performed a first IR stimulation temperature plateau test to check the dependency of $pIRIR_{290}$ D_e values on the first stimulation temperature. Here, we also applied the pIRIR SAR protocol with different first stimulation temperature for our samples to determine D_e (**Table 2**; e.g., Buylaert *et al*., 2012; Yi *et al*., 2016). To construct a dose–response curve, the intensities were derived from the integral of the first 2.0 s (20 channels) after subtracting the average intensity during the last 20 s. The Analyst Version 4.31.9 (Duller, 2016) was used to calculate each D_e. The D_e at each stimulation temperature was determined by calculating the arithmetic mean and standard error of the aliquots (**Fig. 3b**). Most D_e values plotted around the average, except at the first IR stimulation temperature of 250°C for gsj13-039, which showed a large scatter.

A dose recovery test was performed using at least six aliquots from each sample. Aliquots were exposed for 3 h to artificial sunlight in a UVACUBE 400 chamber (Hönle) with a SOL 500 lamp module at a lamp-to-

Table 2. *Single aliquot regenerative (SAR) protocol used for D_e measurements.*

Step	Measurement Protocol	
1	Give dose	
2	Preheat 320°C for 60 s	
3	IRSL 50, 100, 150, 200, 250°C for 200 s	
4	IRSL 290°C for 200 s ($pIRIR_{50/290}$, $pIRIR_{100/290}$, $pIRIR_{150/290}$, $pIRIR_{200/290}$, $pIRIR_{250/290}$)	L_x
5	Give test dose	
6	Preheat 320°C for 60 s	
7	IRSL 50, 100, 150, 200, 250°C for 200 s	
8	IRSL 290°C for 200 s ($pIRIR_{50/290}$, $pIRIR_{100/290}$, $pIRIR_{150/290}$, $pIRIR_{200/290}$, $pIRIR_{250/290}$)	T_x
9	Hot IR bleach for 200 s at 325°C	
10	Return to step 1	

sample distance of 50 cm. After this bleaching, half of the aliquots were given a dose of β-radiation nearly equal to each D_e value and then analyzed, and the remaining aliquots were directly measured to estimate the residual dose. These residual dose values were subtracted from the recovered doses. The arithmetic means of the dose recovery ratio and residual doses were calculated, and the uncertainty was represented as one standard error. The data are shown in **Fig. 3c**. The dose recovery ratios plotted within ±10% from unity, except at the first IR stimulation temperature of 250°C for gsj13-094.

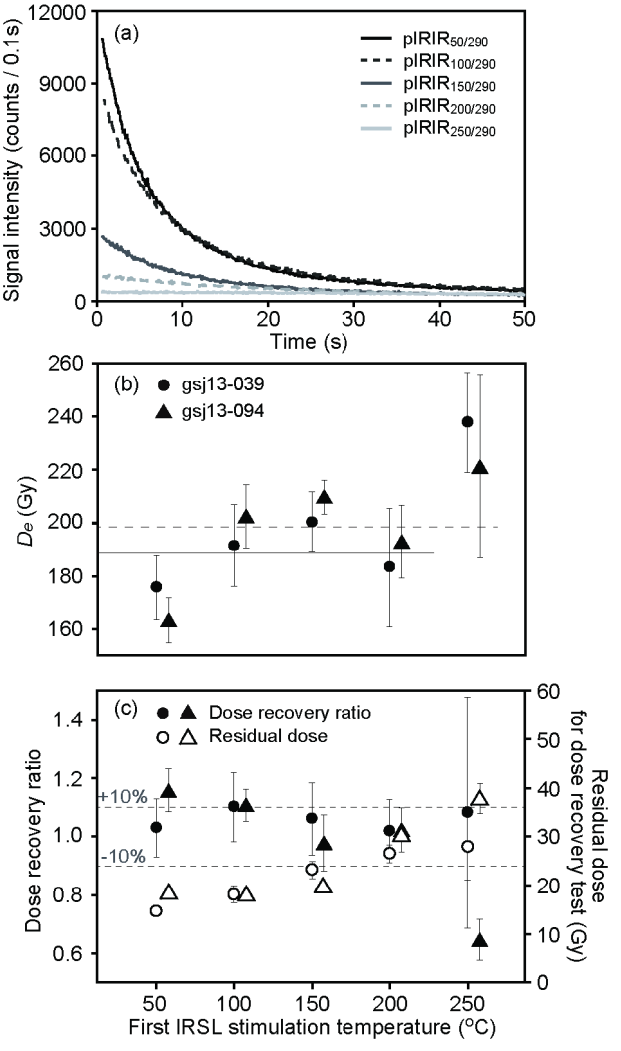

Fig. 3. *pIRIR signal characteristics of samples gsj13-039 and gsj13-094 with different first IR stimulation temperatures. The pIRIR stimulation and preheat temperatures were fixed at 290 and 320°C, respectively. (a) Typical signal intensities of $pIRIR_{290}$ signals from sample gsj13-039, (b) first IR stimulation temperature plateau, and (c) dose recovery ratio and residual dose after bleaching for 3 h with different first stimulation temperatures. The error bars show one standard error. In (b), the bold and dashed lines represent the average D_e of each sample, except for D_e at the first IR measurement temperature of 250°C for gsj13-039. In (c), the dashed lines represent the ±10% range.*

Anomalous fading measurement

It has been suggested that the fading of the $pIRIR_{290}$ signal is negligible in nature, because in very old samples measured by some studies the natural signal was close to the saturation level (Buylaert *et al.*, 2011; Kars *et al.*, 2012; Thiel *et al.*, 2011b; Thomsen *et al.*, 2011). Stability of the $pIRIR_{290}$ signal has also been inferred from age comparisons with an independent age control (Thiel *et al.*, 2011a; 2015; Zander and Hilgers, 2013). However, in these previous studies, the fading rates of the samples were around 1–1.5%/decade (Buylaert *et al.*, 2012; Thiel *et al.*, 2011b), and it was argued that the measured laboratory fading might be an artifact of the measurement procedure (Buylaert *et al.*, 2012). On the other hand, Li and Li (2012) reported that the fading of the $pIRIR_{50/290}$ signal was not negligible in their samples having a natural D_e range from 250 Gy to 700 Gy, but that fading of $pIRIR_{200/290}$ signal was negligible.

In this study, we performed a fading test with different first IR stimulation temperatures using gsj13-039 and gsj13-094 to check the signal stability of our samples (**Fig. 4**). Additionally, for gsj13-040, gsj13-030, gsj13-093, and gsj13-095, we performed a fading test for $pIRIR_{290}$ with first stimulation temperatures of 50°C and 200°C (**Table 3**). Our fading test protocol was based on Auclair *et al.* (2003). Following the dose (*ca.* 140 Gy) and preheating, the delay times were between 0.3 h and 96 h, and the g-values were calculated following Huntley and Lamothe (2001). To express the g-value, the arbitrary time (t_c) was normalized to 2 days (g_{2days}). The data consisted of about 10 points from each sample, and the uncertainty is reported as one standard error. An example is shown in **Fig. 4a**. For all samples, the g-values of the $pIRIR_{50/290}$ and $pIRIR_{200/290}$ signals ranged from 1.25 ± 0.66%/decade to 2.53 ± 0.31%/decade and from –1.34 ± 0.57%/decade to 1.57 ± 0.40%/decade, respectively. The g-values of the $pIRIR_{50/290}$ signal were larger than those of the $pIRIR_{200/290}$ signal. For other signals, most g-values decreased when the first IR stimulation temperature was higher (**Fig. 4b**). The data were also used to calculate the dimensionless recombination center density ρ' (Huntley, 2006), summarized in **Table 3** for the fading correction following Kars *et al.* (2008).

Residual dose estimation

It is well known that the pIRIR signal is much more difficult to bleach than the IR_{50} signal (e.g., Buylaert *et al.*, 2012; Kars *et al.*, 2014; Sohbati *et al.*, 2012). Additionally, Reimann *et al.* (2015) showed that different pIRIR stimulation temperatures have different rates of bleaching under daylight exposure. In bleaching experiments conducted by these previous studies, the pIRIR signal intensity did not reach an unbleachable residual

Table 3. *Results of pIRIR dating using different first IR stimulation temperatures. n is number of aliquots, ρ' is the dimensionless recombination center density (Huntley, 2006). Residual dose was D_e after artificial sunlight bleaching for 3 h except for modern beach sand (gsj14-019) which was bleached for 800 h. Fading correction was performed based on Kars et al. (2008) and Kars and Wallinga (2009). To calculate the uncorrected ages, residual dose of modern beach sand (gsj14-019) was subtracted from D_e of each sample. D_0 values were calculated based on Wintle and Murray (2006).*
[a] Terrigenous sediments. [b] If the average g-value of samples from site 2 was lower than zero, fading correction would not performed.

Sample	Measurement procedure	n	D_e (Gy)	Fading test			Dose recovery test				Fading-uncorrected Age (ka)	Fading-corrected Age[b] (ka)	D_0 (Gy)
				n	g_{2days} (%/decade)	ρ' / 10^{-6}	n	Dose recovery ratio	n	Residual dose (Gy)			
Site 1													
gsj13-040[a]	$pIRIR_{50/290}$	11	96 ± 3	11	2.19 ± 0.09	2.24 ± 0.10	3	0.93 ± 0.09	3	10 ± 1	59 ± 5	95 ± 9	361
	$pIRIR_{200/290}$	17	120 ± 4	7	–1.02 ± 0.73	–1.11 ± 0.72	3	1.07 ± 0.09	3	12 ± 6	74 ± 7	81 ± 8	251
gsj14-014	$pIRIR_{50/290}$	8	163 ± 8				3	1.16 ± 0.05	3	15 ± 1	99 ± 11	167 ± 20	413
	$pIRIR_{200/290}$	11	192 ± 5				3	1.20 ± 0.10	3	25 ± 1	116 ± 10	127 ± 12	324
gsj14-015	$pIRIR_{50/290}$	8	178 ± 8				3	1.06 ± 0.03	3	12 ± 0	105 ± 10	168 ± 16	724
	$pIRIR_{200/290}$	8	181 ± 6				3	0.81 ± 0.05	3	22 ± 1	106 ± 10	116 ± 11	392
gsj13-039	$pIRIR_{50/290}$	28	176 ± 8	28	1.65 ± 0.18	1.64 ± 0.17	10	1.03 ± 0.10	6	15 ± 0	103 ± 10	177 ± 20	422
	$pIRIR_{100/290}$	12	191 ± 10	12	2.22 ± 0.34	2.22 ± 0.33	9	1.10 ± 0.12	6	18 ± 2	112 ± 12	199 ± 25	424
	$pIRIR_{150/290}$	10	200 ± 7	10	1.65 ± 0.31	1.64 ± 0.31	9	1.06 ± 0.12	6	23 ± 2	118 ± 11	178 ± 17	451
	$pIRIR_{200/290}$	19	183 ± 14	19	0.49 ± 0.46	0.48 ± 0.49	12	1.02 ± 0.11	12	27 ± 2	107 ± 15	117 ± 17	370
	$pIRIR_{250/290}$	9	238 ± 8	9	–0.26 ± 1.07	–0.42 ± 1.15	9	1.08 ± 0.40	6	28 ± 7	139 ± 15	139 ± 15	231
gsj14-031	$pIRIR_{50/290}$	7	163 ± 7				3	1.06 ± 0.05	3	13 ± 1	94 ± 9	159 ± 16	410
	$pIRIR_{200/290}$	9	194 ± 7				3	1.01 ± 0.07	3	25 ± 1	112 ± 12	123 ± 13	298
gsj14-030	$pIRIR_{50/290}$	8	204 ± 5	8	2.53 ± 0.31	2.53 ± 0.32	3	1.04 ± 0.05	3	15 ± 0	116 ± 9	199 ± 17	448
	$pIRIR_{200/290}$	13	214 ± 7	12	1.57 ± 0.40	1.57 ± 0.40	3	0.94 ± 0.17	3	31 ± 1	120 ± 12	133 ± 14	258
gsj14-017	$pIRIR_{50/290}$	8	184 ± 5				3	1.04 ± 0.05	3	16 ± 1	113 ± 9	188 ± 16	514
	$pIRIR_{200/290}$	11	204 ± 11				3	1.02 ± 0.07	3	31 ± 1	125 ± 14	136 ± 15	446
gsj14-029	$pIRIR_{50/290}$	8	183 ± 5				3	0.96 ± 0.04	3	14 ± 1	107 ± 9	181 ± 15	453
	$pIRIR_{200/290}$	10	206 ± 9				3	1.01 ± 0.10	3	21 ± 1	120 ± 13	131 ± 15	339
Site 2													
gsj13-093[a]	$pIRIR_{50/290}$	10	95 ± 2	10	1.25 ± 0.66	1.21 ± 0.66	3	1.09 ± 0.05	3	11 ± 0	64 ± 5	94 ± 8	371
	$pIRIR_{200/290}$	16	127 ± 4	8	–1.34 ± 0.57	–1.43 ± 0.62	3	1.13 ± 0.10	3	21 ± 2	86 ± 8		229
gsj13-094	$pIRIR_{50/290}$	17	163 ± 6	11	2.21 ± 0.42	2.24 ± 0.40	3	1.16 ± 0.07	3	19 ± 1	114 ± 10	173 ± 16	461
	$pIRIR_{100/290}$	6	203 ± 7	6	0.55 ± 0.14	0.58 ± 0.15	3	1.11 ± 0.05	3	18 ± 1	142 ± 13	164 ± 16	420
	$pIRIR_{150/290}$	6	210 ± 4	6	1.50 ± 0.23	1.52 ± 0.25	3	0.98 ± 0.09	3	20 ± 1	147 ± 12	223 ± 18	364
	$pIRIR_{200/290}$	24	193 ± 7	12	–0.11 ± 0.74	–0.20 ± 0.76	3	1.02 ± 0.07	3	31 ± 1	134 ± 14		324
	$pIRIR_{250/290}$	4	221 ± 14	4	0.81 ± 0.57	0.83 ± 0.59	3	0.65 ± 0.07	3	38 ± 3	154 ± 27	202 ± 41	253
gsj13-092	$pIRIR_{50/290}$	7	205 ± 5				3	1.08 ± 0.06	3	17 ± 0	126 ± 10	193 ± 16	507
	$pIRIR_{200/290}$	10	219 ± 3				3	1.02 ± 0.07	3	31 ± 1	134 ± 10		287
gsj13-095	$pIRIR_{50/290}$	8	193 ± 5	8	1.82 ± 0.12	1.82 ± 0.13	3	1.16 ± 0.07	3	12 ± 0	121 ± 10	187 ± 16	450
	$pIRIR_{200/290}$	16	214 ± 4	12	1.40 ± 0.22	1.40 ± 0.23	3	0.97 ± 0.06	3	28 ± 1	134 ± 11		354
gsj13-091	$pIRIR_{50/290}$	8	178 ± 3				3	1.07 ± 0.06	3	16 ± 1	118 ± 9	178 ± 14	532
	$pIRIR_{200/290}$	11	205 ± 5				3	1.13 ± 0.12	3	32 ± 2	136 ± 12		312
gsj13-096	$pIRIR_{50/290}$	8	187 ± 13				3	1.06 ± 0.06	3	11 ± 1	115 ± 15	177 ± 26	442
	$pIRIR_{200/290}$	12	202 ± 7				3	1.15 ± 0.06	3	27 ± 1	123 ± 12		339
Site 3													
gsj14-019	$pIRIR_{50/290}$	12	16 ± 2						3	3 ± 0			
	$pIRIR_{100/290}$	8	14 ± 2										
	$pIRIR_{150/290}$	8	11 ± 1										
	$pIRIR_{200/290}$	15	17 ± 1						3	4 ± 0			
	$pIRIR_{250/290}$	8	26 ± 2										

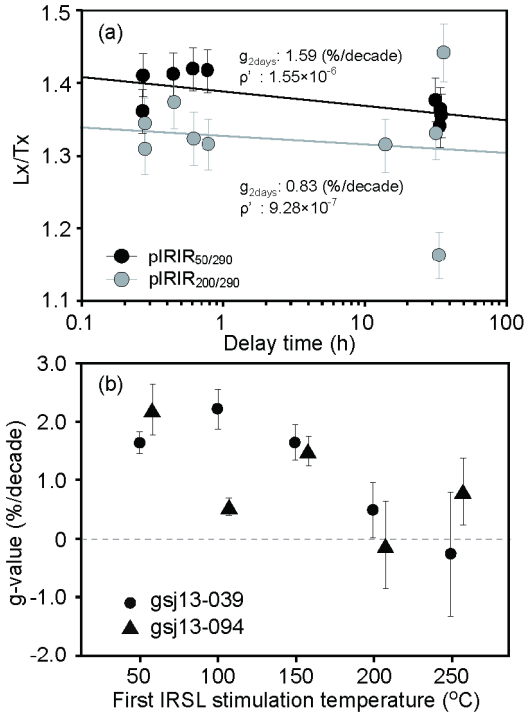

Fig. 4. *Fading test results. (a) Typical results for sample gsj13-039; (b) g-values obtained with different first IR stimulation temperatures for gsj13-039 and gsj13-094. The error bars show one standard error.*

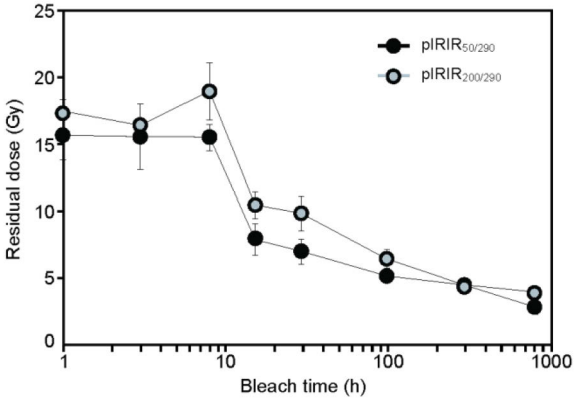

Fig. 5. *Average residual dose obtained for different artificial sunlight bleaching times. Each data point represents the average of at least six aliquots. The error bars show one standard error.*

level. However, Yi *et al.* (2016) recently showed that the residual dose of the pIRIR$_{50/290}$ signal reached a lower limit after artificial sunlight (SOL2) bleaching for 300 h, and its residual dose was 6.2 ± 0.7 Gy. In this study, the D_e of the pIRIR$_{50/290}$ signal of modern beach sand (gsj14-019) was 16 ± 2 Gy (**Table 3**), a much larger value than that of modern beach sand from Oga Peninsula (4.0 ± 0.2 Gy, Buylaert *et al.*, 2012). Since the bleaching of gsj14-019 may have been incomplete, aliquots were bleached under artificial sunlight for longer than 300 h with a maximum bleaching time of 800 h. Sample aliquots were measured using the pIRIR$_{50/290}$ and pIRIR$_{200/290}$ protocols, and the residual dose at each bleaching time was calculated as the average of at least six aliquots with an uncertainty of one standard error (**Fig. 5**). The pIRIR$_{50/290}$ and pIRIR$_{200/290}$ D_e values before bleaching, which were 15.7 ± 1.8 and 17.3 ± 1.0 Gy, respectively, decreased to 2.8 ± 0.2 and 3.9 ± 0.2 Gy, respectively, after 800 h of bleaching. These remaining D_e values were assumed to be the unbleachable residual doses, and they were subtracted from all D_e values used to calculate the pIRIR$_{50/290}$ and pIRIR$_{200/290}$ ages (**Table 3**). For other signals, residual doses after 3 h of bleaching in the dose recovery test increased with the first IR stimulation temperature (**Fig. 3c**). This result indicates that the bleachability of the pIRIR$_{290}$ signal decreases as the first stimulation temperature increases. Therefore, the residual doses of the pIRIR$_{100/290}$, pIRIR$_{150/290}$, and pIRIR$_{250/290}$ signals were inferred by linear interpolation and extrapolation of the pIRIR$_{50/290}$ and pIRIR$_{200/290}$ signals. The assumed residual doses and errors of the pIRIR$_{100/290}$, pIRIR$_{150/290}$, and pIRIR$_{250/290}$ signals were 3.2 ± 0.2, 3.5 ± 0.2, and 4.3 ± 0.2 Gy, respectively.

5. AGES AND DISCUSSION

Fading-uncorrected (residual-subtracted) ages

The fading uncorrected ages obtained with different first IR stimulation temperatures from gsj13-039 and gsj13-094 are shown in **Fig. 6a** and **Table 3**, and those of the pIRIR$_{50/290}$ and pIRIR$_{200/290}$ signals from the samples from the subtidal facies deposits are shown in **Fig. 7**. The uncorrected ages of gsj13-039 with different first IR stimulation temperatures are generally consistent with the expected age (MIS 5e, 123 ± 7 ka), with a possible exception of the pIRIR$_{50/290}$ signal (**Fig. 6a**). On the other hand, the uncorrected gsj13-094 ages of pIRIR$_{100/290}$, pIRIR$_{150/290}$ and pIRIR$_{250/290}$ signals are slightly older than the expected age if we do not consider the large scatter of own age. The uncorrected ages of the pIRIR$_{200/290}$ signals of all samples (**Fig. 7**) were concordant with the expected age. The uncorrected ages of the pIRIR$_{50/290}$ signal from the samples from site 2 were also concordant with the expected age, but the ages of the pIRIR$_{50/290}$ signal from four samples from site 1 were underestimated.

Fading-corrected (residual-subtracted) ages

In the previous section, we showed that fading rates of the pIRIR$_{50/290}$ signal were positive in all samples whereas the fading rates of the pIRIR$_{200/290}$ signal were smaller and consistent with zero in four samples (taking account of the 2-σ uncertainty).

To apply the fading correction, it is necessary to consider the shape of the dose–response curve. If a D_e value

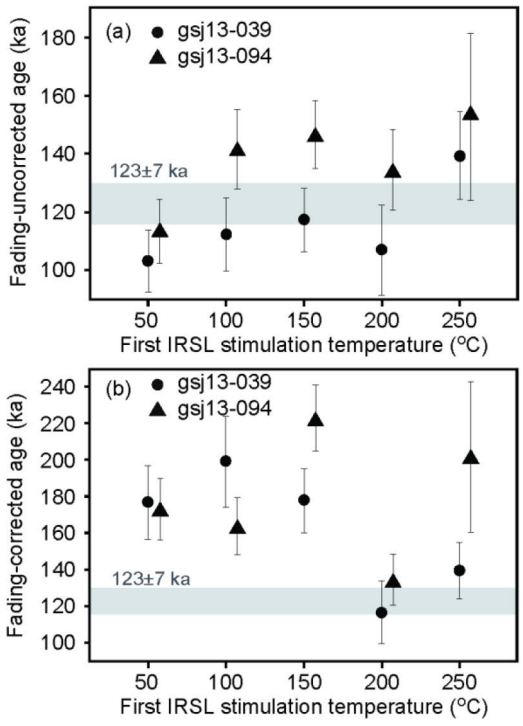

Fig. 6. *(a) Uncorrected and (b) corrected pIRIR ages of gsj13-039 and gsj13-094 obtained with different first IR stimulation temperatures. The error bars show one standard error.*

is within a linear region of the curve, the method of Huntley and Lamothe (2001) can be applied, but if it is on a non-linear part, the method of Kars *et al.* (2008) must be applied. For our samples, all natural signal to natural test dose (L_n/T_n) ratios lay on a non-linear part of the dose–response curve (**Fig. 8**). Therefore, the fading correction was performed by the method of Kars *et al.* (2008) and Kars and Wallinga (2009). This fading correction methods is based on the model of the quantum-mechanical tunnelling process proposed by Huntley (2006). The fading-corrected ages were calculated by plotting measured L_n/T_n on the modelled growth curve, which was obtained from the measured dose–response curve, the the dimensionless recombination center density ρ', and the dose rate. The dimensionless value ρ' was calculated by fitting equation (7) of Huntley (2006) to the fading test results. The attempt-to-escape frequency s was fixed at 3×10^{15} s^{-1} following Huntley (2006). In the fading tests of gsj13-039 and gsj13-094 with different first IR stimulation temperatures, ρ' ranged from $(-0.42 \pm 1.15) \times 10^{-6}$ to $(2.22 \pm 0.33) \times 10^{-6}$ and from $(-0.20 \pm 0.76) \times 10^{-6}$ to $(2.24 \pm 0.40) \times 10^{-6}$, respectively. To calculate the fading-corrected ages of the $pIRIR_{50/290}$ and $pIRIR_{200/290}$ signals, the average value of ρ' was used for each sampling site: $(2.12 \pm 0.26) \times 10^{-6}$ and $(0.34 \pm 0.75) \times 10^{-6}$, respectively, for site 1 (gsj13-040, gsj13-039 and gsj14-030), and $(1.76 \pm 0.30) \times 10^{-6}$ and $(-0.02 \pm 0.79) \times 10^{-6}$, respectively, for site 2 (gsj13-093, gsj13-094 and gsj13-095). For the $pIRIR_{100/290}$, $pIRIR_{150/290}$, and $pIRIR_{250/290}$ signals, the ρ' values of gsj13-039 and gsj13-094 were used for the fading correction.

The corrected ages are shown in the same way as the uncorrected ages (**Figs. 6b** and **7**). Except for the $pIRIR_{200/290}$ signals, the corrected ages with different first IR stimulation temperatures overestimated the expected age. The corrected ages of the $pIRIR_{200/290}$ signals of samples from site 1, like the uncorrected ages of the $pIRIR_{200/290}$ signals of all samples, were concordant with the expected age (**Fig. 7**). On the other hand, the corrected ages of the $pIRIR_{50/290}$ signals from all samples were always older than the expected age. The characteristic saturation dose (D_0) values of our dose–response curves were calculated based on Wintle and Murray (2006) (**Table 3**). The resultant D_0 values, generally ranging between 300 and 500 Gy, were lower than the D_0 values of $pIRIR_{50/225}$ and $pIRIR_{50/290}$ signals reported by Li *et al.* (2017) (500-730 Gy), which were obtained from the dose response curve to the saturation level. Though the size of the regenerative doses in this study were adequate to estimate a reliable D_e value, these low $2D_0$ values were calculated from the dose–response curve which was not constructed up to saturation level. Therefore, to estimate a reliable corrected age of the $pIRIR_{50/290}$ signal, the dose–response curve used for the fading correction should have been extended to saturation level.

Discussion

In this study, both fading-uncorrected and -corrected $pIRIR_{200/290}$ ages in site 1 were shown to be in agreement with the expected age. When we compared the uncorrected and corrected $pIRIR_{200/290}$ ages, the corrected ages showed a much narrower age cluster around the expected age of 123 ± 7 ka, presumably because of a small fading influence. We conclude that the fading-corrected $pIRIR_{200/290}$ ages are most suitable, if a positive ρ' value is calculated.

The fading-corrected and -uncorrected ages of the $pIRIR_{200/290}$ signals of our terrigenous samples (gsj13-040 and gsj13-093) were 81 ± 8 ka and 86 ± 8 ka, respectively, whereas the corrected ages of the samples from the subtidal facies ranged from 116 ± 11 ka to 136 ± 15 ka. The field evidence showed that the terrigenous sediments accumulated after the deposition of the subtidal facies and were separated from them by an erosional surface. These ages indicate that the terrigenous sediment was deposited during MIS 5a. In the samples from the subtidal facies, we found no systematic stratigraphic trend of the $pIRIR_{200/290}$ ages. This concentration of ages of the $pIRIR_{200/290}$ signal is similar to previous results from the Oga Peninsula for the $pIRIR_{50/225}$ signal (Thiel *et al.* 2015). The mean $pIRIR_{200/290}$ ages from the subtidal facies of site 1 and site 2 were calculated to be 126 ± 3 ka and 132 ± 2 ka, respectively.

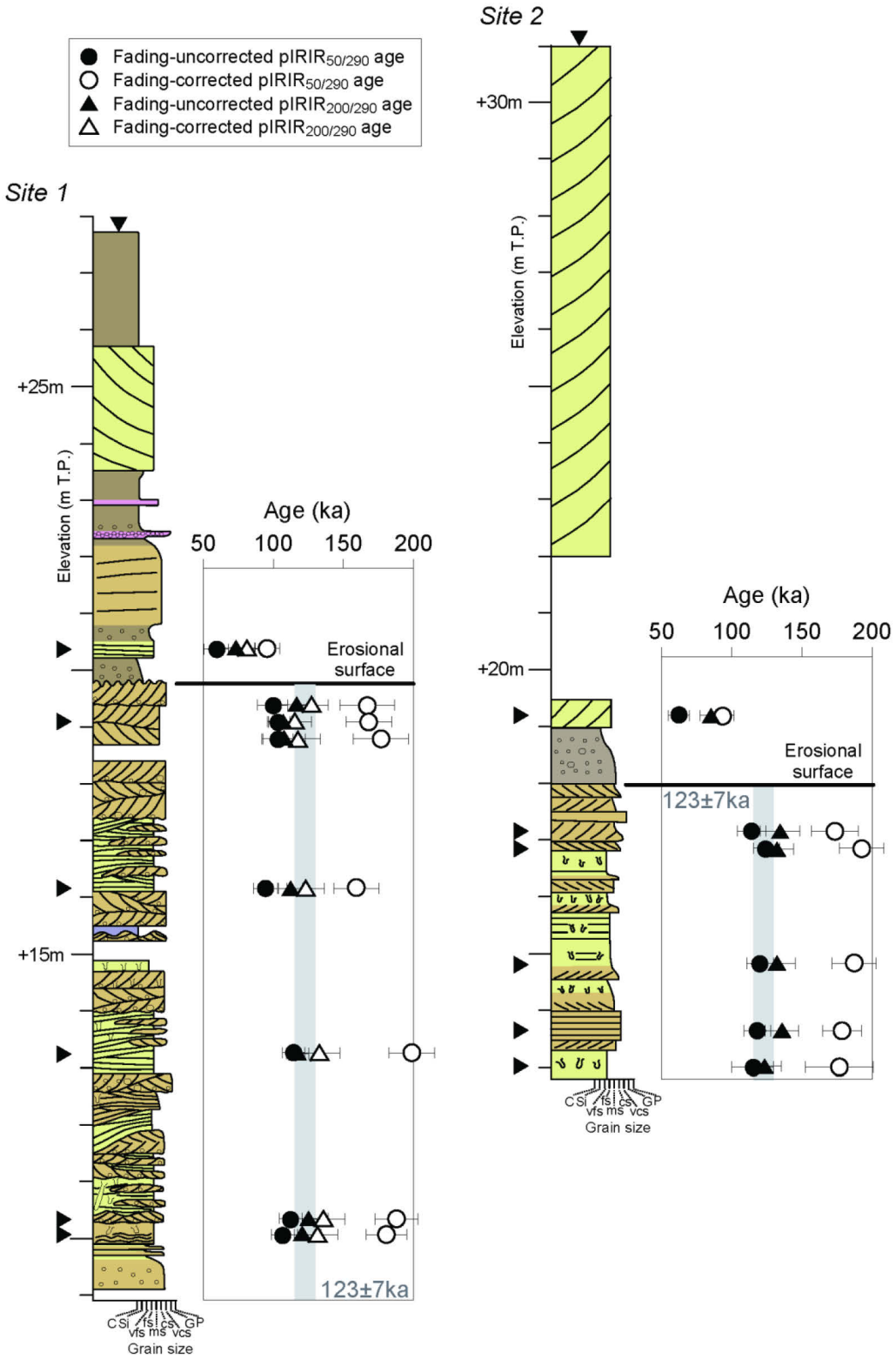

Fig. 7. *Columnar sections as in Fig. 2. For sites 1 and 2, the fading-uncorrected and -corrected ages of the pIRIR$_{50/290}$ and pIRIR$_{200/290}$ signals are shown with one standard error. For site 2, the fading corrected ages of pIRIR$_{200/290}$ signals were not calculated because the average ρ' value was lower than zero. For each site, the vertical gray bar shows the expected age range. T.P. (Tokyo Peil) is the standard datum for elevation measurements in Japan.*

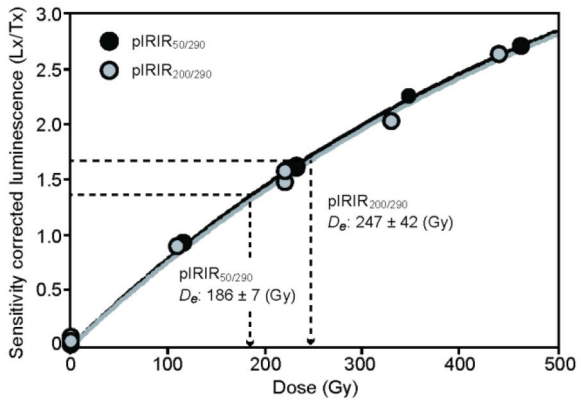

Fig. 8. *Typical dose–response curve for the pIRIR$_{50/290}$ and pIRIR$_{200/290}$ signals of sample gsj13-039.*

6. CONCLUSION

The pIRIR dating protocol was applied to marine terrace deposits from the last interglacial on the Kamikita coastal plain, northeastern Japan. To calculate fading-uncorrected ages, the residual dose that was obtained by bleaching of a modern beach sample for 800 h in a solar simulator was subtracted from the D_e of each sample. With regard to the stability of the pIRIR signal, the g-values decrease as a function of first IR stimulation temperature; from 2%/decade at 50°C to near zero for the pIRIR$_{200/290}$ and pIRIR$_{250/290}$ signals. For site 1, the fading-corrected ages of the pIRIR$_{200/290}$ signals showed a much narrower age cluster around the expected age of MIS 5e; the average corrected age (±1 standard error) was 126 ± 3 ka. On the other hand, for site 2, the fading correction was not necessary because the average ρ' value was lower than zero and the signal was stable; the average uncorrected age was 132 ± 2 ka. We conclude that the pIRIR$_{200/290}$ protocol is most suitable for determining reliable ages of marine terrace deposits of the Kamikita plain. This robust dating protocol can be further applied to determine the ages of not only terraces formed during substages of MIS5 (5a, 5c) but also those of older marine terraces, for which age evidence is limited.

ACKNOWLEDGMENTS

We thank Dr. Georgina King for valuable comments, which helped to improve our paper. This research project was conducted as regulatory supporting research funded by the Secretariat of the Nuclear Regulation Authority, Japan.

REFERENCES

Aitken MJ, 1985. *Thermoluminescence dating*. Academic Press, London.

Aitken MJ, 1998. *An Introduction to Optical Dating*. Oxford, Oxford University Press: 267pp.

Aoki K, 2008. Revised age and distribution of *ca.* 87 ka Aso-4 tephra based on new evidence from the northwest Pacific Ocean. *Quaternary International* 178: 10–118, DOI 10.1016/j.quaint.2007.02.005.

Aoki K, Irino T and Oba T, 2008. Late Pleistocene tephrostratigraphy of the sediment core MD01-2421 collected off the Kashima coast, Japan. *The Quaternary Research* 47: 391–407 (in Japanese, English abstract).

Auclair M, Lamothe M and Huot S, 2003. Measurement of anomalous fading for feldspar IRSL using SAR. *Radiation Measurements* 37: 487–492, DOI 10.1016/S1350-4487(03)00018-0.

Balescu S and Lamothe M, 1994. Comparison of TL and IRSL age estimates of feldspar coarse grains from waterlain sediments. *Quaternary Science Reviews* 13: 437–444, DOI 10.1016/0277-3791(94)90056-6.

Barreto AMF, Bezerra FHR, Sugio K, Tatumi SH, Yee M, Paiva RP and Munita CS, 2002. Late Pleistocene marine terrace deposits in northeastern Brazil: sea-level change and tectonic implications. *Palaeogeography, Palaeoclimatology, Palaeoecology* 179: 57–69, DOI 10.1016/S0031-0182(01)00408-4.

Bell WT, 1980. Alpha dose attenuation in quartz grains for thermoluminescence dating. *Ancient TL* 12: 4–8.

Buylaert JP, Murray AS, Thomsen KJ and Jain M, 2009. Testing the potential of an elevated temperature IRSL signal from K-feldspar. *Radiation Measurements* 44: 560–565, DOI 10.1016/j.radmeas.2009.02.007.

Buylaert JP, Thiel C, Murray AS, Vandenberghe DAG, Yi S and Lu H, 2011. IRSL and post-IR IRSL residual doses recorded in modern dust samples from the Chinese loess plateau. *Geochronometria* 38: 432–440, DOI 10.2478/s13386-011-0047-0.

Buylaert JP, Jain M, Murray AS, Thomsen KJ, Thiel C and Sohbati R, 2012. A robust feldspar luminescence dating method for Middle and Late Pleistocene sediments. *Boreas* 41: 435–451, DOI 10.1111/j.1502-3885.2012.00248.x.

Buylaert JP, Murray AS, Gebhardt AC, Sohbati R, Ohlendorf C, Thiel C, Wastegard S, Zolitschka B and The PASADO Science Team, 2013. Luminescence dating of the PASADO core 5022-1D from Laguna Potrok Aike (Argentina) using IRSL signals from feldspar. *Quaternary Science Reviews* 71: 70–80, DOI 10.1016/j.quascirev.2013.03.018.

Buylaert JP, Yeo E-Y, Thiel C, Yi S, Stevens T, Thompson W, Frechen M, Murray A and Lu H, 2015. A detailed post-IR IRSL chronology for the last interglacial soil at the Jingbian loess site (northern China). *Quaternary Geochronology* 30: 194–199, DOI 10.1016/j.quageo.2015.02.022.

Choi JH, Murray AS, Jain M, Cheong CS and Chang HW, 2003. Luminescence dating of well-sorted marine terrace sediments on the southeastern coast of Korea. *Quaternary Science Reviews* 22: 407–421, DOI 10.1016/S0277-3791(02)00136-1.

Clifton HE, 2006. A reexamination of facies models for clastic shorelines, In: Posamentier H. W., Walker R. G. (Eds.), *Facies Models Revisited*. Society for Sedimentary Geology, Oklahoma, SEPM Special Publication 84: 293–337.

Cummings DI, Dumas S and Dalrymple RW, 2009. Fine-grained versus coarse-grained wave ripples generated experimentally under large-scale oscillatory flow. *Journal of Sedimentary Research* 79: 83–93, DOI 10.2110/jsr.2009.012.

Duller GAT, 1992. Luminescence chronology of raised marine terraces, South-West North Island, New Zealand. *A thesis submitted in fulfilment of the award of the degree of Doctor of Philosophy at the University of Wales*, 1–147.

Duller GAT, 2016. Analyst v4.31.9 user manual, 88p.

Fruergaard M, Andersen TJ, Nielsen LH, Johannessen PN, Aagaard T and Pejrup M, 2015. High-resolution reconstruction of a coastal

barrier system: impact of Holocene sea-level change. *Sedimentology* 62: 928–969, DOI 10.1111/sed.12167.

Ganzawa Y and Ike M, 2011. SAR-RTL dating of single grain of volcanic quartz from the late Pleistocene Toya Caldera. *Quaternary Geochronology* 6: 42–49, DOI 10.1016/j.quageo.2010.07.001.

Guérin G, Mercier N and Adamiec G, 2011. Dose-rate conversion factors: update. *Ancient TL* 29: 5–8.

Huntley DJ, 2006. An explanation of the power-law decay of luminescence. *Journal of Physics: Condensed Matter* 18: 1359–1365, DOI 10.1088/0953-8984/18/4/020.

Huntley DJ and Baril MR, 1997. The K content of the K-feldspars being measured in optical dating or in thermoluminescence dating. *Ancient TL* 15: 11–13.

Huntley DJ and Lamothe M, 2001. Ubiquity of anomalous fading in K-feldspars and the measurement and correction for it in optical dating. *Canadian Journal of Earth Science* 38: 1093–1106, DOI 10.1139/e01-013.

Huntley DJ, Godfrey-Smith DI and Haskell EH, 1991. Light-induced emission spectra from some quartz and feldspars. *Nuclear Tracks and Radiation Measurements* 18: 127–131, DOI 10.1016/1359-0189(91)90104-P.

Jacobs Z, 2008. Luminescence chronologies for coastal and marine sediments. *Boreas* 37: 508–535, DOI 10.1111/j.1502-3885.2008.00054.x.

Kars RH and Wallinga J, 2009. IRSL dating of K-feldspar: Modeling natural dose response curve to deal with anomalous fading and trap competition. *Radiation Measurements* 44: 594–599, DOI 10.1016/j.radmeas.2009.03.032.

Kars RH, Wallinga J and Cohen KM, 2008. A new approach towards anomalous fading correction for feldspar IRSL dating – test on samples in field saturation. *Radiation Measurements* 43: 786–790, DOI 10.1016/j.radmeas.2008.01.021.

Kars RH, Busschers FS and Wallinga J, 2012. Validating post IR-IRSL dating on K-feldspars through comparison with quartz OSL ages. *Quaternary Geochronology* 12: 74–86, DOI 10.1016/j.quageo.2012.05.001.

Kars RH, Reimann T, Ankjærgaard C and Wallinga J, 2014. Bleaching of the post-IR IRSL signal: new insights for feldspar luminescence dating. *Boreas* 43: 780–791, DOI 10.1111/bor.12082.

Koike K and Machida H, 2001. *Atlas of Quaternary Marine Terraces in the Japanese Islands*. University of Tokyo Press, ISBN 4130607359 (in Japanese).

Kuwabara, 2009. Environmental change and its correlation to terraces based on phytolith assemblage of tephra-soil succession after the latter half of the middle Pleistocene drilled at the Kamikita Plain, NE Japan. *The Quaternary Research* 48: 405–416 (in Japanese, English abstract).

Li B and Li SH, 2011. Luminescence dating of K-feldspar from sediments: A protocol without anomalous fading correction. *Quaternary Geochronology* 6: 468–479, DOI 10.1016/j.quageo.2011.05.001.

Li B and Li SH, 2012. A reply to the comments by Thomsen *et al.* on "Luminescence dating of K-feldspar from sediments: A protocol without anomalous fading correction". *Quaternary Geochronology* 8: 49–51, DOI 10.1016/j.quageo.2011.10.001.

Li B, Roberts RG, Jacobs Z and Li S-H, 2014. A single-aliquot luminescence dating procedure for K-feldspar based on the dose-dependent MET-pIRIR signal sensitivity. *Quaternary Geochronology* 20: 51–64, DOI 10.1016/j.quageo.2013.11.001.

Li Y, Tsukamoto S, Frechen M and Gabriel G, 2017. Timing of fluvial sedimentation in the Upper Rhine Graben since the Middle Pleistocene: constraints from quartz and feldspar luminescence dating. *Boreas*, 10.1111/bor.12266.

Lisiecki L and Raymo ME, 2005. A Pliocene-Pleistocene stack of 57 globally distributed benthic $\delta^{18}O$ records. *Paleoceanography* 20: PA1003, DOI 10.1029/2004PA001071.

Machida H and Arai F, 2003. *Atlas of Tephra in and Around Japan*. University of Tokyo Press, ISBN 4130607456 (in Japanese).

Matsu'ura T, Furusawa A, Shimogama K, Goto N and Komatsubara J, 2014. Late Quaternary tephrostratigraphy and cryptotephrostratigraphy of deep-sea sequences (Chikyu C9001C cores) as tools for marine terrace chronology in NE Japan. *Quaternary Geochronology* 23: 63–79, DOI 10.1016/j.quageo.2014.06.001.

Mejdahl V, 1979. Thermoluminescence dating: beta-dose attenuation in quartz grains. *Archaeometry* 21: 61–72, DOI 10.1111/j.1475-4754.1979.tb00241.x.

Miyauchi T, 1985. Quaternary crustal movements estimated from deformed terraces and geologic structures of the Kamikita coastal plain, Northeast Japan. *Geographical Reviews of Japan* 58: 492–515. (in Japanese, English abstract)

Miyauchi T, 1987. Quaternary Tectonic Movements of the Kamikita Coastal Plain, Northeastern Japan. *Geographical Review of Japan* 60: 1–19.

Murray AS and Funder S, 2003. Optically stimulated luminescence dating of a Danish Eemian coastal marine deposit: a test of accuracy. *Quaternary Science Reviews* 22: 1177–1183, DOI 10.1016/S0277-3791(03)00048-9.

Pascucci V, Sechi D and Andreucci S, 2014. Middle Pleistocene to Holocene coastal evolution of NW Sardinia (Mediterranean Sea, Italy). *Quaternary International* 328–329: 3–20, DOI 10.1016/j.quaint.2014.02.018.

Pawley SM, Bailey RM, Rose J, Moorlock BSP, Hamblin RJO, Booth SJ and Lee JR, 2008. Age limits on Middle Pleistocene glacial sediments from OSL dating, north Norfolk, UK. *Quaternary Science Reviews* 27: 1363–1377, DOI 10.1016/j.quascirev.2008.02.013.

Pedoja K, Dumont JF, Lamothe M, Ortlieb L, Collot J-Y, Ghaleb B, Auclair M, Alvarez V and Labrousse B, 2006a. Plio-Quaternary uplift of the Manta Peninsula and La Plata Island and the subduction of the Carnegie Ridge, central coast of Ecuador. *Journal of South American Earth Sciences* 22: 1–21, DOI 10.1016/j.jsames.2006.08.003.

Pedoja K, Ortlieb L, Dumont JF, Lamothe M, Ghaleb B, Auclair M and Labrousse B, 2006b. Quaternary coastal uplift along the Talara Arc (Ecuador, Northern Peru) from new marine terrace data. *Marine Geology* 228: 73–91, DOI 10.1016/j.margeo.2006.01.004.

Prescott JR and Hutton JT, 1994. Cosmic ray contributions to dose rates for luminescence and ESR dating: large depths and long-term time variations. *Radiation Measurements* 23: 497–500, DOI 10.1016/1350-4487(94)90086-8.

Reimann T, Notenboom PD, De Schipper MA and Wallinga J, 2015. Testing for sufficient signal resetting during sediment transport using a polymineral multiple-signal luminescence approach. *Quaternary Geochronology* 25: 26–36, DOI 10.1016/j.quageo.2014.09.002.

Roberts HM, 2012. Testing Post-IR IRSL protocols for minimising fading in feldspars, using loess with independent chronological control. *Radiation Measurements* 47: 716–724, DOI 10.1016/j.radmeas.2012.03.022.

Shirai M, Tada R and Fujioka K, 1997. Identification and Chronostratigraphy of Middle to Upper Quaternary Marker Tephras Occurring in the Anden Coast Based on Comparison with ODP Cores in the Sea of Japan. *The Quaternary Research* 36: 183–196 (in Japanese, English abstract).

Shiraishi T, Arai F and Fujimoto Y, 1992. Discovery of Aso-4 and Drift Pumice of Aso-4 Pyroclastic Flow and Sambe-Kisuki Pumice Fall Deposits in the Upper Quaternary of the Oga Peninsula, Akita Prefecture, Northeast Honshu, Japan. *The Quaternary Research* 31: 21–27 (in Japanese, English abstract).

Sohbati R, Murray AS, Buylaert JP, Ortuño M, Cunha PP and Masana E, 2012. Luminescence dating of Pleistocene alluvial sediments affected by the Alhama de Murcia fault (eastern Betics, Spain) – a comparison between OSL, IRSL and post-IR IRSL ages. *Boreas* 41: 250–262, DOI 10.1111/j.1502-3885.2011.00230.x.

Tamura T, Nanayama F, Saito Y, Murakami F, Nakashima R and Watanabe K, 2007. Intra-shoreface erosion in response to rapid sea-level fall: depositional record of a tectonically uplifted strand plain, Pacific coast of Japan. *Sedimentology* 54: 1149–1162, DOI 10.1111/j.1365-3091.2007.00876.x.

Tanaka K, Hataya R, Spooner NA, Questiaux DG, Saito Y and Hashimoto T, 1997. Dating of marine terrace sediments by ESR, TL and OSL methods and their applicabilities. *Quaternary Science Reviews* 16: 257–264, DOI 10.1016/S0277-3791(96)00092-3.

Thiel C, Coltorti M, Tsukamoto S and Frechen M, 2010. Geochronology for some key sites along the coast of Sardinia (Italy). *Quaternary International* 222: 36–47, DOI 10.1016/j.quaint.2009.12.020.

Thiel C, Buylaert JP, Murray AS and Tsukamoto S, 2011a. On the applicability of post-IR IRSL dating to Japanese loess. *Geochronometria* 38: 369–378, DOI 10.2478/s13386-011-0043-4.

Thiel C, Buylaert JP, Murray AS, Terhorst B, Hofer I, Tsukamoto S and Frechen M, 2011b. Luminescence dating of the Stratzing loess profile (Austria) – Testing the potential of an elevated temperature post-IR IRSL protocol. *Quaternary International* 234: 23–31, DOI 10.1016/j.quaint.2010.05.018.

Thiel C, Buylaert JP, Murray AS, Elmejdoub N and Jedoui Y, 2012. A comparison of TT-OSL and post-IR IRSL dating of coastal deposits on Cap Bon peninsula, north-eastern Tunisia. *Quaternary Geochronology* 10: 209–217, DOI 10.1016/j.quageo.2012.03.010.

Thiel C, Tsukamoto S, Tokuyasu K, Buylaert J P, Murray AS, Tanaka K and Shirai M, 2015. Testing the application of quartz and feldspar luminescence dating to MIS 5 Japanese marine deposits. *Quaternary Geochronology* 29: 16–29, DOI 10.1016/j.quageo.2015.05.008.

Thomsen KJ, Murray AS, Jain M and Bøtter-Jensen L, 2008. Laboratory fading rates of various luminescence signals from feldspar-rich sediment extracts. *Radiation measurements* 43: 1474–1486, DOI 10.1016/j.radmeas.2008.06.002.

Thomsen KJ, Murray AS and Jain M, 2011. Stability of IRSL signals from sedimentary K-feldspar samples. *Geochronometria* 38: 1–13, DOI 10.2478/s13386-011-0003-z.

Walker RG and Plint AG, 1992. Wave and storm-dominated shallow marine systems, In Walker R.G. and James N.P. (Eds.), *Facies Models response to Sea-Level Change*. Geological Assn of Canada: 219–238.

Wintle AG and Murray AS, 2006. A reviews of quartz optically stimulated luminescence characteristics and their relevance in single-aliquot regeneration dating protocols. *Radiation Measurements* 41: 369–391, DOI 10.1016/j.radmeas.2005.11.001.

Yi S, Buylaert JP, Murray AS, Lu H, Thiel C and Zeng L, 2016. A detailed post-IR IRSL dating study of the Niuyangzigou loess site in northeastern China. *Boreas* 45: 644–657, DOI 10.1111/bor.12185.

Zander A and Hilgers A, 2013. Potential and limits of OSL, TT-OSL, IRSL and pIRIR290 dating methods applied on a Middle Pleistocene sediment record of Lake El'gygytgyn, Russia. *Climate of the Past* 9: 719–733, DOI 10.5194/cp-9-719-2013.